Metamaterial inspired terahertz devices: from ultra-sensitive sensing to near field manipulation

Jin Wang (王 锦)[1,2], Shuang Wang (王 爽)[1,2*], Ranjan Singh[3], and Weili Zhang (张伟力)[2]**

[1] *School of Electronic Engineering, Tianjin University of Technology and Education, Tianjin 300222, China*

[2] *School of Electrical and Computer Engineering, Oklahoma State University, Stillwater, Oklahoma 74078, USA*

[3] *AOT-HPE, Los Alamos National Laboratory, Los Alamos, NM87545, USA*

[*] *Corresponding author: wshuang@okstate.edu;* [**] *Corresponding author: ranjan.ranjansingh@gmail.com*

Received December 13, 2012; accepted December 28, 2012; posted online January 6, 2013

We present a review of terahertz plasmonic metamaterial devices that have functionalities and applications ranging from sensing, enhanced electromagnetic fields, and near field manipulation. Metamaterials allow the properties of light propagation to be manipulated at will by using a combination of appropriately designed geometry and suitable materials at the unit cell level. In this review, we first discuss the sensing aspect of a planar plasmonic metamaterial and how to overcome its limitations. Conventional symmetric metamaterials are limited by their low Q factor, thus we probed the symmetry broken plasmonic metamaterial structures in which the interference between a broad continuum mode and a narrow localized mode leads to the excitation of the sharp Fano resonances. We also discuss the near field mediated excitation of dark plasmonic modes in metamaterials that is caused by a strong coupling from the bright mode resonator. The near field coupling between the dark and bright mode resonances leads to classical analogue of electromagnetically induced transparency in plasmonic systems. Finally, we discuss active switching in terahertz metamaterials based on high temperature superconductors that holds the promise of reducing the resistive losses in these systems, though it fails to suppress the radiation loss in plasmonic metamaterial at terahertz frequencies.

OCIS codes: 160.3918, 300.6495.

doi: 10.3788/COL201311.011602.

1. Introduction

The past decade has seen tremendous advances in the plasmonics and metamaterials research[1−6]. This particular field involves researchers from several different areas, including physics, engineering, and material science, interested in fabricating as well as synthesizing subwavelength structures with novel geometries and optical properties. Applications such as developing novel molecular sensing schemes and creating high speed miniaturized circuits have been proposed and demonstrated. Many of these applications are inspired by unique electromagnetic properties of metamaterials which are mainly derived from the localized resonance modes supported in these artificially designed structures. These localized resonances create sharp spectral absorption and scattering peaks as well as enhanced electromagnetic near fields[7−15]. The intense electromagnetic field generated at the metamaterial resonances, its high sensitivity to the environment of the resonators, and the inter-particle coupled interactions are at the heart of many of the applications. Here, in this article we present an overview of terahertz plasmonic metamaterials with applications and functionalities as a sensor[17−20], a Fano resonator[12−15,21−28], near field coupling effect[12−15,22,23,29−39], and an active superconductor device[41−48].

2. Terahertz time-domain spectroscopy and sample fabrication

Broadband THz time-domain spectroscopy (THz-TDS) configured in transmission arrangement was employed to investigate the electromagnetic properties of metamaterials[16]. Details of our THz-TDS are described in Ref. [48]. In the transmission measurements, a blank slab identical to the array substrate was used as a reference. The transmitted terahertz electric field through the sample and reference was recorded in time domain and then Fourier transformed into frequency-dependent amplitude spectra as $E_{\rm s}$ (ω) and $E_{\rm r}$ (ω), respectively. The absolute amplitude transmission of the array was defined as $t(\omega) = |E_{\rm s}(\omega)/E_{\rm r}(\omega)|$ and the corresponding phase change was obtained through the relation, $\varphi(\omega) = \arg[t(\omega)]$.

A general procedure was followed to fabricate all the samples that were planar metallic split ring resonator (SRR) structures on silicon substrate[5]. The patterns shown in Fig. 1 were fabricated by use of conventional photolithography and metallization processes on high-quality silicon (0.64 mm thick, p-type resistivity $\rho = 20$ Ω·cm or $\rho = 12$ Ω·cm) substrate. A 200-nm-thick Al metal film formed the SRRs.

3. Sensing with plasmonic metamaterials

In this section, We focus primarily on metamaterial plasmonic sensors. The simplest sensing application of plasmonic metamaterials is to detect changes in the bulk refractive index of their environment through shifts in the resonances supported by metamaterials[17−20]. The most common fundamental resonance in SRR metamaterials is the inductive-capacitive (LC) resonance which is excited due to the asymmetry of the split ring structure with the incident electric field. Figure 2 displays the spectra of amplitude transmission measurements of SRRs when a

planar array is coated with different thicknesses of photo resist material (0, 1.5, 4, 8, and 16 μm)[17]. The refractive index of the photoresist is ~1.64 at 1.0 THz. The resonance shift saturates when the film thickness is increased up to 16 μm. The SRR array used for sensing is shown in Fig. 1. As the thickness of the film changes from 1.5 to 16 μm, the LC resonance frequency is tuned from 0.446 to 0.424 THz. To further explore the redshift behavior of the SRRs, even thicker dielectric layers were applied. However, when the film thicknesses varied from 16 to 90 μm, no additional frequency shift was observed. To explore the response sensitivity of SRRs to the ultrathin dielectric layers, a B_2O_3 film ($\varepsilon_2 = 3.6 \pm 0.2$ at 1.0 THz) as thin as 100 nm is thermally evaporated on the surface of the SRR array and a frequency shift of about 2–3 GHz was observed. The reason for the red-shift in the resonance is the capacitive effect. Capacitors are formed in the splits of the SRRs and the gap between the inner and outer rings. In addition to the silicon substrate, the over layer combines with air and serves as an effective second boarding medium on the other side of metal. The boarding media on both sides of the SRRs make contributions to the capacitors. Furthermore, the overlayer fills the splits and the gap between the rings. The value of capacitance is proportional to the relative permittivity of the capacitor medium. Thus, a shift in the LC resonance towards lower frequencies occurs due to increase in the effective capacitance as $\omega_{LC} \propto (LC)^{-1/2} \propto (\varepsilon_{eff})^{-1/2}$, where ε_{eff} is the effective dielectric constant that includes contributions of the boarding media on both sides of the SRRs.

A metamaterial array based on a high-permittivity substrate will have a large and likely majority, capacitive contribution in the substrate. Obviously, the sensed layer cannot penetrate the substrate or interact with any of the electric flux contained therein. This substantially dilutes the change in capacitance and decreases the amount of resonance shift due to the overlayer. Though thinner substrates or sharper resonances would certainly improve the situation, it is clear from the saturated resonance shift data in Fig. 2 that substrate of only 10-20 μm is sufficient to maximize this dilution effect. As the SRR fringing field was extending out to roughly 16 μm, electric flux is not contained directly within the SRR gaps[17]. As such, any sensed layer confined to the gaps would have no interaction with this fringing flux, thus reducing its effect on the measured resonance. Thus, we

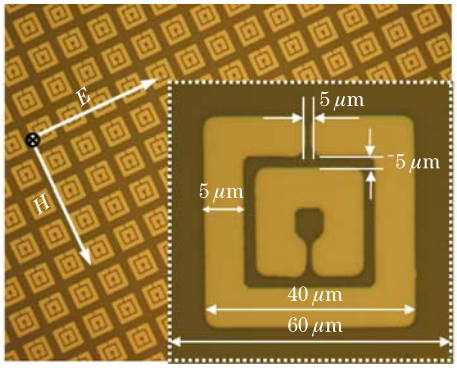

Fig. 1. Microscopic images of planar metallic SRRs. Inset: geometrical dimensions of a SRR unit cell.

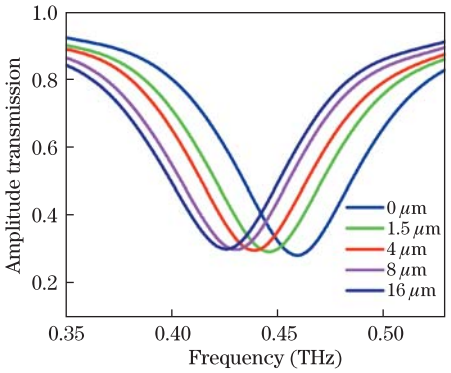

Fig. 2. (Color online) Measured amplitude transmission spectra with overlayer dielectric film of 0, 1.5, 4, 8, and 16 μm thicknesses spin-coated on SRRs.

show that metamaterial arrays can indeed act as label free sensors.

4. High Q plasmonic Fano resonances in terahertz metamaterials

A Fano resonance in a periodic plasmonic metamaterial media could be defined as an asymmetric subradiant lineshaped resonance that is formed due to interference between a broad continuum resonance mode and a narrow highly localized resonance mode. Exciting Fano resonances in metamaterials has led to an extremely sharp asymmetric resonance profile that has immensely helped in curbing the radiative losses in plasmonic systems at microwave, terahertz, and optical frequencies[12–15,21–28]. In the previous section, we reviewed the sensing aspect of metamaterials by measuring the shift in the LC resonance frequency. The smallest shift in frequency is limited by the linewidth of the metamaterial resonance. By exploiting the Fano resonances, it is possible to measure the tiny shifts in the resonance frequency due to its ultra-high quality (Q) factor, thus facilitating ultrasensitive sensing. We will now describe how to excite these narrow resonances in a terahertz metamaterial[12–15].

The inset of Fig. 3 shows the two gap asymmetric split ring resonator (ASR) structure consisting of two pieces of metallic wires of different lengths. The top wire formed an angle of 170° and the bottom one with 150°[12]. Another sample with perfect symmetry was designed for comparison with top and bottom wires forming equal angles of 160° and we called this a symmetric split ring resonator (SSR). Figure 3 shows the transmission measurement results of the SSR and ASR metamaterials. The most striking difference between the transmission curves of the two metamaterial array is the sharp asymmetric Fano resonance dip in the ASRs excited at 0.86 THz while the incident electric field is oriented perpendicular to the gaps. The SSR sample shows only one broad symmetric resonance at 1.18 THz[12].

Looking at the simulated surface currents at the Fano resonance frequency (0.86 THz) in the left hand side inset of Fig. 3, we observe anti-parallel currents in the top and bottom arcs. As the structure is only weakly coupled to the free space these currents are very strong and pronounced. This particular Fano resonance mode

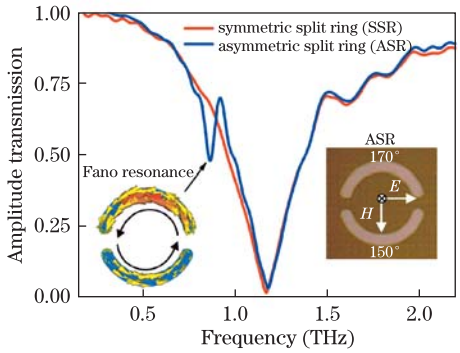

Fig. 3. (Color online) Measured amplitude transmission spectra for symmetric and asymmetric split ring arrays with the E-field orientation perpendicular to the gap. The left inset shows the simulated surface currents at the sharp Fano resonance, and the right inset shows microscope image of an asymmetric split ring unit cell.

is similar in nature to the LC resonance in a single gap SRR as both resonances result in current configurations that give rise to a magnetic dipole moment perpendicular to the plane of the array. The Q factor of the Fano resonance measured in Fig. 3 is about 17 and can reach much higher values if the asymmetry parameter is kept minimum[14]. The high Q asymmetric resonance in the ASR mainly arises from the structural asymmetry which leads to an interference between a sharp discrete resonance and a much broader continuum-like spectrum of dipole resonance. This narrow resonance arises from a subradiant dark mode for which the radiation losses are completely suppressed due to the weak coupling of the structure to free space. Such dark modes are exploited to realize the electromagnetically induced transparency (EIT)-like effects in metamaterials which open up avenues for designing slow light devices with high group index. The broad symmetric resonance at 1.18 THz is due to a dipole-like parallel current distribution in the top and the bottom arcs. These dipole resonances are strongly coupled to free space and, hence, are rather broad due to their highly radiative nature.

Hence, ASR Fano plasmonic metamaterials with a weak asymmetry are likely to hold potential for the use in notch filters. Small changes in the local environment of the asymmetric metamaterial supporting the Fano resonance would induce dramatic resonance shifts and help the design of ultrasensitive sensors. The Fano metamaterials also open the route towards tunable devices which could be based on the circular dichroism of terahertz waves mediated through a chiral arrangement of the planar asymmetric metamaterial with respect to the incident terahertz field[25].

5. Near-field coupling between bright and dark plasmonic modes in metamaterials

Manipulation of the near field is a challenging task since it does not radiate efficiently away from the scattering objects. The importance of near field should be stressed due to the fact that it contains the finer details of the object from which it scatters. The emergence of metamaterials that has the ability to support resonances in subwavelength structures created the possibility to capture and control electromagnetic near fields in artificially designed structures[12−15,22,23,29−37]. In this section we review a near field mediated coupling between bright and dark mode metamaterial resonators[12−15,29,30].

The near field coupled metamaterial arrays are shown in Figs. 4(a) and 4(b)[29]. The unit cell of each meta molecule comprised of two SRRs as shown in Fig. 4(c). The bright resonator is directly excited by the incident electric field of linearly polarized terahertz radiation along the split gap and the dark resonator is excited via near field coupling from the bright resonator. From the measurement results shown in Fig. 5, we clearly observe a strong coupling between the bright and the dark plasmonic eigenmodes[29]. Their interaction becomes possible because at a relative rotation by 90° the orientation of both SRRs breaks the overall symmetry of the coupled structure. This broken symmetry renders the excitation of the otherwise forbidden dark mode possible. We studied two scenarios where we probed the effect of separation between the dark and bright mode SRR in order to change their coupling strengths. The separation between the SRRs was defined by a parameter 's'. In Fig. 5, we measured the transmission spectra in the case of the two SRRs being weakly coupled ($s = 3$ μm) and strongly coupled ($s = 0$ μm). We could clearly see the difference in their behavior[29]. The weakly coupled SRRs showed a weak splitting of their resonance whereas the strongly coupled SRRs had a very sharp transparency peak analogous to EIT in quantum physics[13−15,29−35].

Due to their coupled nature the eigenmodes of SRRs themselves are not excitable but rather a polaritonic state. For large spectral detuning of both resonances the excitation of the dark mode is rather weak. The closer the resonance frequencies get the stronger is the excitation of the dark mode. Similarly, the excited eigenmodes deviate from the spectral position of the eigenmodes for the isolated SRRs. Anticrossing causes a strong spectral separation of the bright and dark mode from their

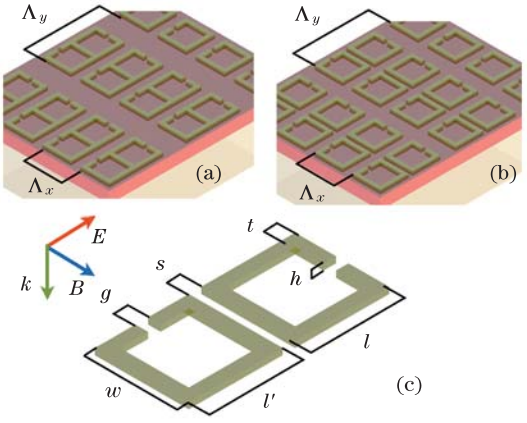

Fig. 4. Principal sketch of near-field coupled metamaterial arrays where (a) $s = 0$ and (b) $s = 3$ μm. (c) Detailed definition of the geometrical parameters of the unit cell where $s = 3$ μm. The parameters are chosen to be $t = 6$ μm, $g = 2$ μm, $l' = w = l = 36$ μm, $h = 200$ nm, $s = 0$ or 3 μm. The periodicity of the unit cells in all samples is $\Lambda_x = 50$ μm by $\Lambda_y = 100$ μm. The left hand side SRR is the bright resonator and on the right hand side is the dark resonator.

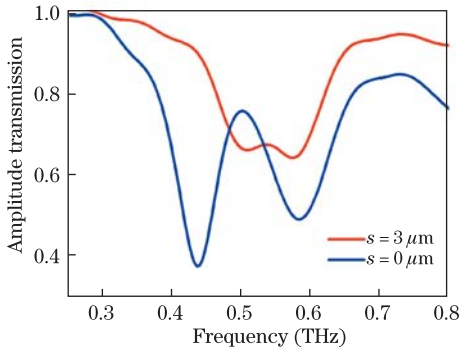

Fig. 5. (Color online) Measured amplitude transmission spectra of a weakly coupled ($s = 3$ μm) and strongly coupled ($s = 0$ μm) bright and dark mode SRRs.

spectral position in the unperturbed situation. We observe the excitation of a polaritonic state. A Rabi splitting of the energetic levels is experimentally observed and numerically verified for the case of the two touching SRRs. Such strong splitting renders the observed spectra to be similar to an Autler-Townes-type doublet. The weak coupling seems to be insufficient to induce sudden spectral changes, as one would expect in the case of a truly EIT analogy. The reduced coupling is caused by the reduced spatial overlap of the eigenmodes. That means, if both modes couple, a spectral splitting occurs, leading to the formation of a symmetric and anti-symmetric mode. Finally the magnitude of the splitting depends on the near-field coupling strength between the eigenmodes. Thus, the symmetry broken metamaterials allow manipulation of near-field coupling between the eigenmodes.

6. Active superconductor metamaterial

Metals provide high conductivity to realize a strong resonant response in metamaterials but they contribute very little to the tunability[40]. The integration of semiconductors or complex oxides into metal resonators allows designing tunable metamaterials by a change of environment using an external stimulus[39−48]. The complex conductivity of high-temperature superconducting films is highly sensitive to external perturbations, which provides new opportunities in achieving tunable metamaterials resulting directly from the resonant elements. Additionally, superconducting metamaterials are expected to enable strong nonlinear response and quantum metamaterials. In this section we review thermal tuning of resonance in $YBa_2Cu_3O_{7-\delta}$ (YBCO) SRR arrays. The imaginary part of the complex conductivity increases by orders of magnitude upon phase transition and consequently the metamaterial resonance switches in amplitude.

The superconductor metamaterial sample shown in the inset Fig. 6 was lithographically fabricated from a commercially available 280-nm-thick YBCO film, which typically has $T_c = 86$ K and a critical current of 2.3 MA/cm^2 grown on a 500-μm thick sapphire substrate (THEVA, Germany)[41]. The measured transmission spectra, as shown in Fig. 6 reveal the switching effect in the SRR LC resonance upon cooling the sample from room temperature to well below the superconducting T_c at 27 K[41]. The superconductor undergoes a huge change in its conductivity after reaching the superconducting phase transition temperature. According to the two-fluid model, the real part of the YBCO conductivity is contributed by the normal state carriers whose motion follows Drude model while the imaginary part is determined by the superconducting carriers. It should be noted that the conductivity due to Cooper pairs is purely imaginary and thus the resistivity of the YBCO below T_c is also nearly imaginary, resulting in an inductor type behavior under the applied terahertz field. In the terahertz regime, at temperatures higher than T_c the real part of conductivity is dominant since the absolute value of the imaginary conductivity is three orders of magnitude less than the real part. However, starting from several Kelvins under T_c the imaginary conductivity value rises drastically with falling temperatures and the total conductivity is then dominated by the imaginary part. The temperature-dependent amplitude modulation achieved at the LC resonance is nearly absent in the regular metamaterial composed of thin metal films as the conductivity of metals cannot be modified as that of a superconductor. Thus superconductors are unique to metamaterial applications since they allow active thermal tuning as well as having the potential to overcome the Joule losses in metamaterial and plasmonic structures[42−45].

7. Perspective and future directions

The future outlook for terahertz metamaterials still includes numerous fundamental studies, but now there seems to be a sufficient foundation for a more dedicated application oriented pursuit, beyond simple filters and planar resonators. The artificially designed and actively controlled metamaterial structures supporting sharp resonances open the door to new levels of electromagnetic control, to better leverage the inherent advantages of metamolecules. While the terahertz has traditionally been a difficult operating range, it is arguably the most susceptible to major technological improvements by these novel ideas and approaches that are based on

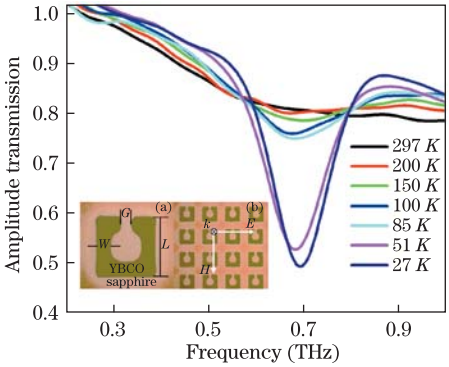

Fig. 6. (Color online) Measured amplitude transmission spectra of the active superconductor metamaterial at low temperatures. The inset (a) shows microscopic image of superconductor metamaterial unit cell with structural parameters, $W = 8$ μm, $G = 5$ μm, and $L = 32$ μm and (b) shows superconductor metamaterial array with a periodicity of $P = 52$ μm. The incident E field is polarized parallel to the gap of the SRRs.

metadevices. Future technologies require tremendous increase in photonic integration of metamaterial based devices that would open up the avenues for competing with high speed electronics. Terahertz metamaterials hold the promise to bridge this gap between electronics and photonics with plethora of opportunities to develop the next generation metamaterial and plasmonic active and passive devices.

The authors would like to thank John F. O'Hara, Ibraheem Al-Naib, Carsten Rockstuhl, Jianquang Gu, Zhen Tian, Jiaguang Han, and Wei Cao for their outstanding contributions to this study. This work was partially supported by the US National Science Foundation.

References

1. J. B. Pendry, A. J. Holden, D. J. Robbins, and W. J. Stewart, IEEE Trans. Microwave Theory Technol. **47,** 2075 (1999).
2. R. A. Shelby, D. R. Smith, and S. Schultz, Science **292,** 5514 (2001).
3. T. J. Yen, W. J. Padilla, N. Fang, D. C. Vier, D. R. Smith, J. B. Pendry, D. N. Basov, and X. Zhang, Science **303,** 1494 (2004).
4. S. Linden, C. Enkrich, M. Wegener, J. Zhou, T. Koschny, and C. M. Soukolis, Science **306,** 1351 (2004).
5. A. K. Azad, J. M. Dai, and W. Zhang, Opt. Lett. **31,** 634 (2006).
6. W. J. Padilla, A. J. Taylor, C. Highstrete, M. Lee, and R. D. Averitt, Phys. Rev. Lett. **96,** 107401 (2006).
7. R. Singh, E. Smirnova, A. J. Taylor, J. F. O'Hara, and W. Zhang, Opt. Express **16,** 6537 (2008).
8. R. Singh, A. K. Azad, J. F. O'Hara, A. J. Taylor, and W. Zhang, Opt. Lett. **33,** 1506 (2008).
9. M. Walther, A. Ortner, H. Meier, U. Loffelmann, P. J. Smith, and J. G.Korvink, Appl. Phys. Lett. **95,** 251107 (2009).
10. R. Singh, E. Plum, C. Menzel, C. Rockstuhl, A. K. Azad, R. A. Cheville, F. Lederer, W. Zhang, and N. I. Zheludev, Phys. Rev. B **80,** 153104 (2009).
11. S. Zhang, Y. S. Park, J. Li, X. Lu, W. Zhang, and X. Zhang, Phys. Rev. Lett. **102,** 23901 (2009).
12. R. Singh, I. A. I. Al-Naib, M. Koch, and W. Zhang, Opt. Express **19,** 6312 (2011).
13. R. Singh, I. A. I. Al-Naib, Y. Yang, D. Roy Chowdhury, W. Cao, C. Rockstuhl, T. Ozaki, R. Morandotti, and W. Zhang, Appl. Phys. Lett. **99,** 201107 (2011).
14. W. Cao, R. Singh, I. A. I Al-Naib, M. He, A. J. Taylor, and W. Zhang, Opt. Lett. **37,** 3366 (2012).
15. J. Gu, R. Singh, X. Liu, X. Zhang, Y. Ma, S. Zhang, S. A Maier, Z. Tian, A. K. Azad, H.-T. Chen, A. J. Taylor, J. Han, and W. Zhang, Nat. Commun. **3,** 1151 (2012).
16. D. Grischkowsky, S. Keiding, M. van Exter, and Ch. Fattinger, J. Opt. Soc. Am. B **7,** 2006 (1990).
17. J. F. O'Hara, R. Singh, I. Brener, E. Smirnova, J. Han, A. J. Taylor, and W. Zhang, Opt. Express **16,** 1786 (2008).
18. I. A. I. Al-Naib, C. Jansen, and M. Koch, Appl. Phys. Lett. **93,** 083507 (2008).
19. S. -Y. Chiam, R. Singh, J. Gu, J. Han, W. Zhang, and A. A. Bettiol, Appl. Phys. Lett. **94,** 064102 (2009).
20. S.-Y. Chiam, R. Singh, W. Zhang, and A. A. Bettiol, Appl. Phys. Lett. **97,** 191906 (2010).
21. B. Luk'yanchuk, N. I. Zheludev, S. A. Maier, N. J. Halas, P. Nordlander, H. Giessen, and C. T. Chong, Nat. Mater. **9,** 707 (2010).
22. R. Singh, X. Lu, J. Gu, Z. Tian, and W. Zhang, J. Opt. **12,** 015101 (2010).
23. R. Singh, C. Rockstuhl, and W. Zhang, Appl. Phys. Lett. **97,** 241108 (2010).
24. R. Singh, I. A. I. Al-Naib, M Koch, and W Zhang, Opt. Express **18,** 13044 (2010).
25. R. Singh, E. Plum, W. Zhang, and N. I. Zheludev, Opt. Express **18,** 13425 (2010).
26. Y. Yang, R. Huang, L. Cong, Z. Zhu, J. Gu, Z. Tian, R. Singh, S. Zhang, J. Han, and W. Zhang, Appl. Phys. Lett. **98,** 121114 (2011).
27. I. Al-Naib, R. Singh, C. Rockstuhl, F. Lederer, S. Delprat, D. Rocheleau, M. Chaker, T. Ozaki, and R. Morandotti, Appl. Phys. Lett. **101,** 071108 (2012).
28. S. Zhang, D. A. Genov, Y. Wang, M. Liu, and X. Zhang, Phys. Rev. Lett. **101,** 047401 (2008).
29. R. Singh, C. Rockstuhl, F. Lederer, and W. Zhang, Phys. Rev. B **79,** 085111 (2009).
30. S. -Y. Chiam, R. Singh, C. Rockstuhl, F. Lederer, W. Zhang, and A. A. Bettiol, Phys. Rev. B **80,** 153103 (2009).
31. N. Papasimakis, V. A. Fedotov, N. I. Zheludev, and S. L. Prosvirnin, Phys. Rev. Lett. **101,** 253903 (2008).
32. R. Singh, C. Rockstuhl, F. Lederer, and W. Zhang, Appl. Phys. Lett. **94,** 021116 (2009).
33. Z. Li, Y. Ma, R. Huang, R. Singh, J. Gu, Z. Tian, J. Han, and W. Zhang, Opt. Express **19,** 8912 (2011).
34. Y. Ma, Z. Li, Y. Yang, R. Huang, R. Singh, S. Zhang, J. Gu, Z. Tian, J. Han, and W. Zhang, Opt. Mater. Express **1,** 391 (2011).
35. X. Liu, J. Gu, R. Singh, Y. Ma, J. Zhu, Z. Tian, M. He, J. Han, and W. Zhang, Appl. Phys. Lett. **100,** 131101 (2012).
36. G. Kumar, S. Pandey, A. Cui, and A. Nahata, New J. Phys. **13,** 033024 (2011).
37. G. Kumar, A. Cui, S. Pandey, and A. Nahata, Opt. Express **19,** 1072 (2011).
38. R. Singh, Z. Tian, J. Han, C. Rockstuhl, J. Gu, and W. Zhang, Appl. Phys. Lett. **96,** 071114 (2010).
39. J. Gu, R. Singh, Z. Tian, W. Cao, Q. Xing, M. He, J. W. Zhang, J. Han, H.-T. Chen, and W. Zhang. Appl. Phys. Lett. **97,** 071102 (2010).
40. Z. Tian, R. Singh, J. Han, J. Gu, Q. Xing, J. Wu, and W. Zhang, Opt. Lett. **35,** 3586 (2010).
41. R. Singh, A. K. Azad, Q. X. Jia, A. J. Taylor, and H.-T. Chen, Opt. Lett. **36,** 1230 (2011).
42. B. B. Jin, C. Zhang, S. Engelbrecht, A. Pimenov, J. Wu, Q. Xu, C. Cao, J. Chen, W. Xu, L. Kang, and P. Wu, Opt. Express **18,** 17504 (2010).
43. R. Singh, J. Xiong, A. K. Azad, H. Yang, S. A Trugman, Q. X. Jia, A. J. Taylor, and H.-T. Chen, Nanophotonics **1,** 117 (2012).
44. D. R. Chowdhury, R. Singh, J. F. O' Hara, H. –T. Chen, A. J. Taylor, and A. K. Azad, Appl. Phys. Lett. **99,** 231101 (2011).
45. J. Gu, R. Singh, A. K. Azad, J. Han, A. J. Taylor, J. F. O'Hara, and W. Zhang, Opt. Mater. Express **2,** 1617 (2011).
46. W. Zhang, Eur. Phys. J. Appl. Phys. **43,** 1 (2008).
47. D. R. Chowdhury, R. Singh, M. Reiten, J. Zhou, A. J. Taylor, and J. F. O'Hara, Opt. Express **19,** 10679 (2011).
48. D. R. Chowdhury, R. Singh, M. Reiten, H. T. Chen, A. J. Taylor, J. F. O'Hara, and A. K. Azad, Opt. Express **19,** 15817 (2011).